On lateral mixing efficiency of lunar regolith

Lin Li[1] and John F. Mustard

Department of Geological Sciences, Brown University, Providence, Rhode Island, USA

Received 14 May 2004; revised 14 July 2005; accepted 3 August 2005; published 15 November 2005.

[1] To reexamine the potential for lateral mixing over large distances (>100 km) by impact craters, a mathematical model utilizing the stable probability distribution is proposed for estimating lateral mixing efficiency on the Moon. The proposed model divides material mixing into shallow slope and steep slope regimes. Mixing in the shallow slope regime conforms to the condition that the exponent of the power law describing lunar crater size frequency is larger than the exponent of the power law describing the rim thickness plus 2; otherwise the mixing is called the steep slope regime. The model suggests that in the shallow slope regime, lateral mixing on the Moon is efficient enough to deliver 20–30% exotic components over distances greater than 100 km (e.g., highland material to the mare). The model indicates that lateral mixing conforming to the steep slope regime is not efficient if linear addition of ejecta deposits is assumed because in this regime, impact cratering is driven by small craters reworking lunar surface, and the addition of crater ejecta is an invalid assumption. If the result of the proposed model for the shallow slope regime is applied to regolith layers below the reworked zone, a significant number of "exotic" components is predicted.

Citation: Li, L., and J. F. Mustard (2005), On lateral mixing efficiency of lunar regolith, *J. Geophys. Res.*, *110*, E11002, doi:10.1029/2004JE002295.

1. Introduction

[2] The knowledge of the composition of lunar soils is fundamental for understanding geological processes on the Moon and deciphering the history of lunar evolution. In general, the composition of lunar soils is assumed to be representative of the bedrock beneath. However, most Apollo and Luna samples indicate a significant amount of materials derived from elsewhere [*Wood et al.*, 1970; *Quaide and Oberbeck*, 1975; *Rhodes*, 1977; *Laul and Papike*, 1980; *Laul et al.*, 1981; *Hörz*, 1978; *Hörz et al.*, 1991]. Given the interest in lunar regolith evolution and future sample return missions, it is important to understand the origin of these exotic components [*Li and Mustard*, 2003].

[3] In the Apollo era of lunar exploration impact mixing was introduced as the process responsible for the presence of exotic components, but the relative importance of lateral versus deep vertical mixing was unresolved [*Florenskiy et al.*, 1974; *Evensen et al.*, 1974; *Murthy*, 1975; *Rhodes*, 1977; *Hörz*, 1978]. Here deep vertical mixing refers to the excavation of highland materials beneath an overlying mare deposit, which is distinct from shallow, small-scale vertical mixing describing the regolith turnover and impact gardening by many small craters [*Yingst and Head*, 1999; *Li and Mustard*, 2000]. At the root of the debate on the relative importance of lateral versus deep vertical mixing is the origin of highland components (20–30% by mass) in soil samples returned from several mare regions [*Evensen et al.*, 1974; *Murthy*, 1975; *Quaide and Oberbeck*, 1975; *Rhodes*, 1977; *Hörz*, 1978; *Hörz et al.*, 1991]. One side of the debate proposed that the exotic components come from remote highland regions via lateral mixing, while the other side suggested that they result from deep vertical mixing by "local" craters ranging from a few hundred meters to a few kilometers in diameter [*Evensen et al.*, 1974; *Murthy*, 1975; *Quaide and Oberbeck*, 1975; *Rhodes*, 1977; *Hörz*, 1978; *Hawke et al.*, 2004]. Each side demonstrated the supporting evidence resulting mainly from geochemical and petrographic studies of returned samples, impact cratering modeling and remote sensing observations.

[4] In the past decades, the geochemical analyses of lunar soil samples have provided evidence for efficient vertical mixing [*Adler et al.*, 1974; *Farrand*, 1988; *Simon et al.*, 1981; *Simon et al.*, 1990]. However, most of these studies were limited to modeling soil development and evolution governed by the shallow vertical mixing [e.g., *Arnold*, 1975]. Therefore these argument were less or not relevant to the deep vertical mixing process. *Quaide and Oberbeck* [1975] provided a specific Monte Carlo model that established the fractional contribution to the regolith thickness of crater ejecta as a function of source depth, and the work adequately addressed the deep vertical mixing process. The model, however, predicted that only 5% of the regolith comes from depths of 75 m or more. Because mare basalts were at least several hundred meters thick [*Hörz*, 1978], this model would indicate that an insignificant (<5%) amount of highland had been excavated from beneath basaltic mare via

[1]Now at Department of Geology, Indiana University–Purdue University at Indianapolis, Indianapolis, Indiana, USA.

0148-0227/05/2004JE002295$09.00

deep vertical mixing. Therefore deep vertical mixing was not able to explain the origin of the significant (20–30%) highland contamination observed in mare soils.

[5] As an additional transport mechanism, lateral mixing due to either repetitive impacts or single catastrophic events was also proposed to explain the highland contamination. Several studies have documented "large-scale" lateral mixing through primary crater ejecta (rays) of single large craters on the Moon [*Evensen et al.*, 1974; *Murthy*, 1975; *Pieters et al.*, 1985; *Campbell et al.*, 1992; *Head et al.*, 1993; *Fischer and Pieters*, 1995; *Blewett et al.*, 1995; *Mustard and Head*, 1996; *Staid et al.*, 1996; *Korotev et al.*, 2000; *Korotev and Gillis*, 2001; *Jolliff et al.*, 2000; *Li and Mustard*, 2003]. Specific to lateral transport by repetitive impacts, previous observations and modeling work demonstrated that lateral mixing by repetitive impacts appeared to be efficient only within distances much less than 100 km. *Florenskiy et al.* [1974] showed a 50-km albedo gradient across a mare-highland boundary, suggesting lateral mixing at mare-highland contacts on the Moon occurred. Our recent work [*Mustard et al.*, 1998; *Li and Mustard*, 2000] showed symmetric mixing zones across mare-highland contacts, which were ascribed to lateral mixing by repetitive impacts of many small craters. Our observations indicated efficient mixing only within a short distance (2 to 4 km) from the mare-highland contacts. The models by *Shoemaker et al.* [1969, 1970] and *Arvidson et al.* [1975] also indicated inefficient lateral mixing over a large distance.

[6] The general goal of this paper is to re-examine the potential for efficient lateral mixing over a large distance (>100 km) by impact craters less than 10–20 km in diameter. A new model is proposed to serve this purpose. The new model used a stable distribution to describe regolith thickness. A stable distribution is a family of distributions that allows skewness and heavy tails in a density distribution. The family of this distribution is characterized by *Lévy* [1954] in his study of sums of independent identically distributed (IID) terms. Appendix A provides a brief introduction to the stable distribution law. The new proposed model differs from previous models and has the capability to accommodate a wide range of exponents for the power law describing the crater size frequency distribution. The model by *Arvidson et al.* [1975] used the power law with the exponent 3.4 to describe the crater size frequency, and would diverge when the exponents less than 3 were used. The specific objective of the paper is to show (1) how lateral mixing efficiency depends on the crater ejecta thickness decay and the size frequency distribution and (2) how 20–30% of exotic components across 100 km or more can be likely created by lateral mixing. For a given site, lateral mixing efficiency here refers to the ratio of ejecta from a given distance and beyond to the total accumulative ejecta (TAE) at that site. Throughout the rest of the paper the significant contamination means the introduction of 20–30% of the exotic components, and the critical distance is referred to 100 km.

2. Lateral Mixing Model

[7] *Marcus* [1969, 1970] proposed a model to describe lunar elevation and considered a cratered surface as the "moving average" of a random point process. The model assumed that an initially flat surface is excavated by primary impact craters and a linear superposition of ejecta blankets occurs at any given point of the lunar surface. We adopted this model to estimate lateral mixing efficiency on the Moon. We first specified a site (**o**) on the Moon as the origin of our coordinates (see Appendix B), then calculated the total accumulative ejecta (TAE) at the origin produced by all surrounding craters, and finally derived lateral mixing efficiency. Lateral mixing efficiency is a function of the distances of the craters from the origin (**o**).

2.1. Total Accumulative Ejecta at a Site

[8] Let $N(x, \boldsymbol{r})$ be a Poisson random variable; x represents the crater diameter in meters; $\boldsymbol{r}$ is a vector representing crater location, and r denotes the length of the vector $\boldsymbol{r}$; dN denotes the number of craters of diameter x to x + dx in a small region d($\boldsymbol{r}$) centered at the point **o**. Let $\zeta(x, r)$ denote the blanket thickness of a crater with diameter x and located at $\boldsymbol{r}$. The total accumulative ejecta (TAE) Z, a random variable can then be represented by

$$Z = \int \zeta(x, \mathbf{r}) dN(x, \mathbf{r}) \tag{1}$$

[9] *Marcus* [1970] found that Z obeys a "stable distribution" law. Because of the lack of a closed formula, the probability density of the stable distribution is computed through a Fourier transform (FT). Let $p(Z)$ denote the probability density of Z. Then the characteristic function (CF) corresponding to $p(Z)$, $\phi(u)$ is first obtained through a FT. The FT of $p(Z)$ gives

$$\begin{aligned}\phi(u) &= \int_{-\infty}^{+\infty} \exp(iuz)p(z)dz \\ &= \exp\left(\int_{x_0}^{x_\infty} \xi(x)dx \int_0^{\infty} 2\pi r[\exp(iu\zeta(x,r)) - 1]dr\right),\end{aligned} \tag{2}$$

where x_m and x_0 are the maximum and minimum crater diameters respectively and $\xi(x)$ denotes the expected number of craters of diameter x per unit area per unit diameter interval.

[10] *Marcus* [1970] defined two conditions:

$$\xi(x) = Ff(x) = F\frac{\gamma x_0^\gamma}{1-(x_0/x_m)^\gamma}\frac{1}{x^{\gamma+1}}, \qquad x_0 < x < x_m, \tag{3}$$

$$\begin{aligned}\zeta(x,r) &= R_0 x^h (x/2r)^k, \qquad & r > x/2, \\ &= 0, & r < x/2,\end{aligned} \tag{4}$$

where $F = C/x_0^\gamma$ denotes the total number of craters per unit area (km^2) with diameters $x_0 < x < x_m$; C is a constant; $f(x)$ is the percent frequency of craters with a diameter x relative to total crater population, and it is derived through normalizing differential crater frequency by total crater number ranging from x_0 to x_m in diameter (see section B3 for details); γ is the exponent of the power law describing the crater size

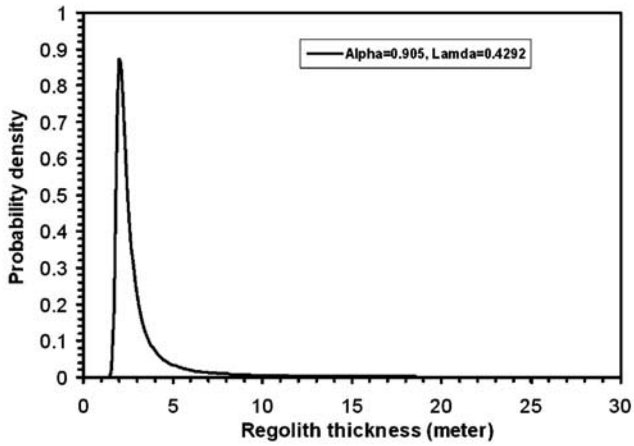

Figure 1. Example probability density of stable distribution. Alpha determines the mode location, and lambda defines the full width of half maximum.

frequency distribution; the coefficient R_0 and the exponent h characterizes the dependence of ejecta thickness at the crater rim on the crater diameter x; and k is an exponent of the power law describing ejecta thickness decay with distance. A detailed derivation of the CF is provided in Appendix B. In the following, we apply equation (B13) to evaluate two regimes of lateral mixing. The expression of the CF can be written as

$$\lim_{\substack{x_0\to 0\\ x_m\to\infty}} \phi(u) = \exp(-\lambda|u|^{\alpha}[1 - i\,\mathrm{sgn}(u)\tan(\pi\alpha/2)]) \tag{5}$$

$$2/k < \alpha = (\gamma - 2)/h < 1$$

$$\lambda = \frac{\pi\gamma R_0^{\alpha} C}{2k\alpha(\gamma - 2 - 2h/k)}\Gamma(1-\alpha)\cos(\pi\alpha/2) \tag{6}$$

where $\Gamma(\cdot)$ is the Gamma function; $i = \sqrt{-1}$; sgn(u) = 1 if u > 0, sgn(u) = −1 if u < 0. For the limits $x_m \to \infty$, and $x_0 \to 0$, the conditions of $2 + 2h/k < \gamma \le 2 + h$ and $k > 2$ must be met. Equation (5) represents the characteristic functions of a stable density distribution [*Gnedenko and Kolmogorov*, 1954]. With a specification of parameters in equation (5), the probability density distribution of the TAE is computed by running STABLE. A brief introduction to STABLE is given in section 4. Figure 1 gives an example of a probability distribution computed with STABLE where α = 0.905 and λ = 0.4292. One observes that a stable density distribution is unimodal and bell shaped [*Zolotarev*, 1986; *Nolan*, 1997]. The mean value for the distribution $p(Z)$ does not exist when $2 + 2\,h/k < \gamma < 2 + h$, the mode of the stable density distribution, is used as an approximate estimate of TAE. The mode scales with $\lambda^{1/\alpha}$, and λ is solved using equation (6).

[11] When $\gamma > 2 + h$, $x_0 \to 0$ is not permitted by the model, and we have to specify the smallest crater diameter. After this modification, instead of the mode of the probability distribution, the mean value of TAE, *E[Z]* can be calculated from equation (B13). *Marcus* [1970] gave

$$E[z] = -i\frac{d}{du}\phi(u)_{u=0} = \frac{\pi\gamma R_0}{2(k-2)(\gamma-2-h)}F x_0^{2+h}. \tag{7}$$

As shown in Table 1, we refer to lateral mixing with $2 + 2\,h/k < \gamma \le 2 + h$ as the shallow slope regime, and with $\gamma > 2 + h$ as the steep slope regime in later discussion. Recall that the slope in a log-log plot of the crater size frequency distribution is determined by the exponent of the corresponding power law (γ). One should also note that $x_m \to \infty$, and $x_0 \to 0$ for the shallow slope regime, and $x_m \to \infty$, and $x > 0$ for the steep slope regime.

2.2. Total Accumulative Ejecta (TAE) From a Given Distance

[12] In order to derive lateral mixing efficiency of the TAE, we derive the TAE delivered from a distance r or more (see Appendix B). Let $p_r(z)$ denote the probability density function of the TAE delivered from sites with the least distance r from the origin. The CF $\phi_r(u)$ corresponding to $p_r(z)$ can be written as (Appendix B)

$$\phi_r(\mu) = \int_{-\infty}^{\infty} e^{i\mu Z} p_r(Z)\,dz$$

$$= \exp\left(\int_{x_0}^{x_m} \xi(x)dx \int_{r}^{\infty} 2\pi r\left[e^{i\mu\varsigma(x,r)}\right] - 1\right)dr. \tag{8}$$

[13] The integration in equation (8) can be evaluated explicitly for $2 + 2\,h/k < \gamma < k + h$ and $k > 2$:

$$\lim_{\substack{x_0\to 0\\ x_m\to\infty}} \phi_r(u) = \exp(-\lambda|u|^{\alpha_r}[1 - i\,\mathrm{sgn}(u)\tan(\pi\alpha/2)]), \tag{9}$$

$$2/k < \alpha_r = \gamma/(k+h) < 1,$$

$$\lambda_r = \frac{\pi\gamma R_0^{(\alpha_r)} C}{2(\alpha_r k)(\gamma - 2 - 2h/k)(2r)^{\alpha_r k - 2}}\Gamma(1-\alpha_r)\cos(\pi\alpha_r/2), \tag{10}$$

[14] Following the similar procedure of deriving $p(Z)$, $p_r(Z)$ can also be derived by STABLE. The mode of the derived density function is used as the estimates of total accumulative ejecta. The mode, scaling with λ_r^{1/α_r} (equation (10)), can be estimated from the probability distribution

Table 1. Lateral Mixing Regimes and Properties

Regime	Property	Examples (h = 1) k = 2.6	k = 3
Shallow slope	$2 + 2\,h/k < \gamma < 2 + h$	$2.77 < \gamma < 3$	$2.67 < \gamma < 3$
Steep slope	$\gamma > 2 + h$	$\gamma > 3$	$\gamma > 3$

Table 2. Parameter Values for the Model

R_0	h	k	γ
0.032	1	2.5	2.81~2.99
0.032	1	2.61	2.77~2.99
0.032	1	3	2.67~2.99

produced by STABLE. The mode of a probability density curve (e.g., Figure 1) is defined as the value of a random variable corresponding to the peak probability density, which is the most representative value for a variable (i.e., total accumulative ejecta).

2.3. Lateral Mixing Efficiency

[15] A more precise formulation for lateral mixing efficiency is likely to be derived if equations (6) and (10) are used. However the result is very lengthy and complicated. We have derived from equation (10) a simplified relationship to express lateral mixing efficiency. The simplified formula is given by

$$Z_r(r) = r^{\varepsilon}, \quad (11)$$

where $\varepsilon = -(k - 2/\alpha_r)$, $r > 1$, $k > 2$, and $\alpha_r = \frac{\gamma}{h+k}$. Equation (11) is derived through three steps: (1) set r = 1 m in equation (10) and calculate the TAE produced by craters formed beyond a 1 m diameter circle, (2) set an arbitrary r (>1 m) and derive the corresponding TAE, and (3) divide the result from the first step by the second for normalization and the final result gives lateral mixing efficiency.

3. Parameter Specification

[16] The calculation of the TAE and lateral mixing efficiency requires the parameter specification for the derived model. Because the parameters describing the ejecta distribution (i.e., R_0, h, and k) and the crater size frequency (i.e., F, C and γ) on the Moon do not have unique values, various combinations of values for these empirical constants are used in this study.

3.1. Ejecta Distributions

[17] As a function of distance from the center of a crater, the ejecta thickness has a maximum at the crater rim, and exhibits power law decay with increasing distances [*McGetchin et al.*, 1973]. One can find a wide range of values for h and R_0 depending upon the scale of craters considered. For large craters and basins on the Moon, the value for h is 0.74 and 1 when the value for R_0 is 0.14 and 0.04, respectively [*McGetchin et al.*, 1973; *Settle and Head*, 1977]. *Pike* [1974] argued that the value for h can take 0.34 for R_0 taking 22.84 or 35.05, 0.343 for R_0 taking 31.1, and 1.0 for R_0 taking 0.033. For small craters the value for h can take 0.94 and R_0 0.10 [*Arvidson et al.*, 1975]. For experimental craters, *Stöffler et al.* [1975] showed that h equals 1 and R_0 0.06. We set R_0 = 0.032 and h = 1, which is appropriate for large craters [*Schultz and Mustard*, 2004]. We chose to use these values because we want to emphasize the contribution of large craters. Given these values for R_0 = 0.032 and h = 1, the ejecta thickness at the rim of a 1-km diameter crater was estimated to be 32 m. If the eject thickness follows a −3 power decay law, this thickness would be estimated to be 4 m at a distance of 1 km from the crater rim, 0.5 m at 2 km, and 0.148 m at 3 km. The exponent k in equation (4) varies with crater diameter (x) and distance from the crater center (r) [*Marcus*, 1970; *Schultz et al.*, 1981; *Housen et al.*, 1983]. For values of k, 3 fits small craters well, and 3 to 5 for large craters [*McGetchin et al.*, 1973; *Melosh*, 1980; *Marcus*, 1970]. k also varies with target characteristics, and is estimated to be 2.61 for impacts into regolith and 3 for solid rock targets [*Housen et al.*, 1983; *Schultz*, 1999]. It has been suggested that k varies as a function of distance, with 4 or 5 near crater rim, to 2 beyond about three crater radii [*Schultz et al.*, 1981]. While it is difficult to incorporate the uncertainties of k into our model, we examined the following values of k: 2.5, 2.61, and 3.

3.2. Crater Size Frequency

[18] The relationship between the crater production frequency (the cumulative number per unit area) and the crater diameter for lunar mare craters is characterized by a double segmentation curve in a log-log plot [*McGill*, 1977; *Wilhelms*, 1987]. The slope of the curve for craters between a few hundred meters and a few kilometers generally ranges between 2 and 3. The slope for craters larger than a few kilometers ranges between 1.8 and 2 [*Baldwin*, 1985; *Chapman and McKinnon*, 1986; *Wilhelms*, 1987]. The dependence of the slope on the crater diameter can be due

Table 3. Regolith Thickness and Slope of Crater Size Frequency at Apollo Stations

Apollo Station	Regolith Thickness, m		Slope	Crater Number (>1 km/km^2)[a]
	Craters	Seismic		
11	3–6[b]	4.4[c]	2.93[d]	$3.4^{+3.6}_{-1.6} \times 10^{-3}$
12	2–4[b]	3.7[c]	2.86[d]	$2.4^{+0.3}_{-0.4} \times 10^{-3}$
14	10–20[e]	8.5[b]	-	-
15	5[b]	4.4[c]	3.55[f]	$2.6^{+0.6}_{-0.4} \times 10^{-3}$
16	3.7–6.7[g]	12.2[b]	-	-
17	3–20[b]	6.2–36.9[b]	3.4[f]	$9.0^{+2.3}_{-3.0} \times 10^{-3}$

[a]*Wilhelms* [1987].
[b]*Watkins and Kovach* [1973].
[c]*Nakamura et al.* [1975].
[d]*Shoemaker et al.* [1970].
[e]*Swann et al.* [1971].
[f]*Neukum et al.* [1975].
[g]*Oberbeck* [1971].

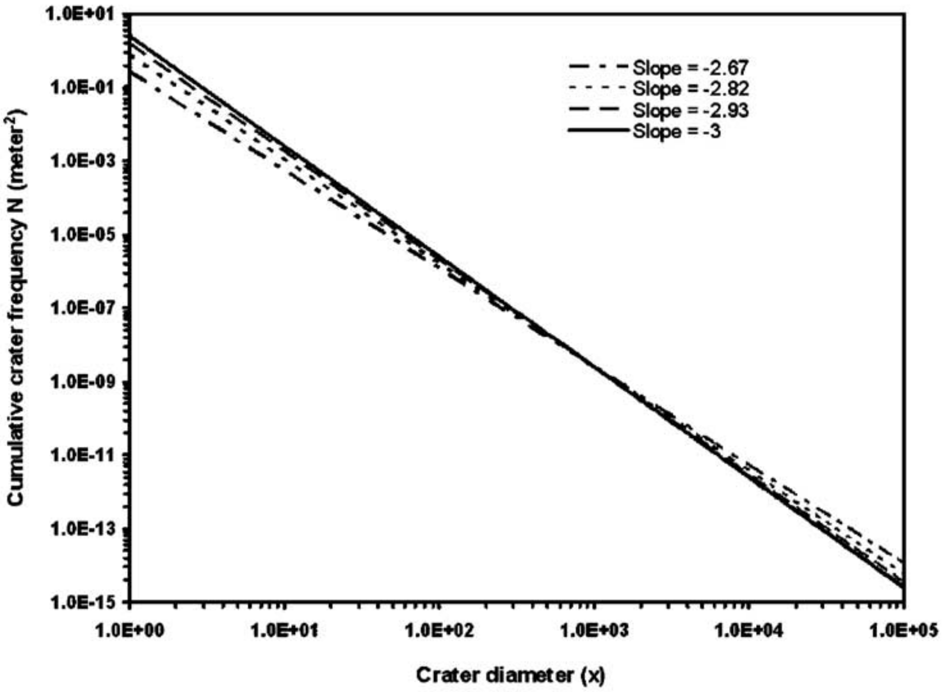

Figure 2. Example of extrapolating cumulative crater frequencies for varying slopes from 1 km diameter downward to 1 m and upward to 10^5 m. The crater number at 10^3 m equals 2.5×10^{-9} per m^2.

to the projectile size frequency distribution, target properties, and the varying scaling relation during impact cratering [*Schultz*, 1988]. It is not possible to use a single slope for all sizes of lunar craters. Nevertheless, we used a single slope (between 3 and 2) in our model in order to emphasize the contribution to the cumulative ejecta of craters between a few hundred meters and a few kilometers in diameter because these craters contributed more ejecta fragments from bedrock than small craters [*Quaide and Oberbeck*, 1975]. We run our model with various combinations of parameters to constrain the uncertainties resulting from using a single slope. For the condition $\gamma > 2 + 2\ h/k$, the shallowest slopes used were 2.67, 2.77, and 2.8 when k = 3, 2.61, and 2.5, respectively. We used a single value 2.99 for the steepest slope when k = 3, 2.61 and 2.5. The values for parameters R_0, h, k, and γ are given in Table 2.

[19] For our calculations, we used a crater density of 2.5×10^{-3} (number per km^2) for upper Imbrian series mare (UISM), and 7.5×10^{-4} (number per km^2) for Copernican mare (CM) [*Wilhelms*, 1987]. These values shown in Table 3 are the cumulative crater density for craters one km or larger in diameter. Given these values we computed the density (the cumulative crater number per m^2) for craters >1 m in diameter given the varying slopes of the crater size frequency distributions. Figure 2 shows an example in which the crater population was extrapolated downward to the number of craters larger than 1 m.

3.3. Crater Size Frequency Correction

[20] The crater size frequency is based on the observed crater diameter statistics, while the scaling law for the ejecta distribution is associated with "apparent" transient crater diameters (precollapse diameter referenced to the target surface before impacts). Therefore two corrections are needed for retrieving the "apparent" transient diameter from the observed rim-rim diameter so that equation (3) can be applied: the first correction to the diameter enlargement due to crater slumping and the second for referring dimensions to the "apparent" transient diameter [*Schultz and Mustard*, 2004].

[21] Let x_{obs}, x_{slc}, and x_a denote the finally observed rim-rim diameter, the slump-corrected diameter, and the "apparent" transient diameter. The following relation was suggested by *Schultz* [1988] for the first correction:

$$x_{obs} = x_{slc} + \Delta x \tag{12}$$

$$x_{slc} = x_{obs} - 0.25 x_a \tag{13}$$

where $\Delta x = 0.25\ x_a$.

[22] *Schultz and Mustard* [2004] suggested the second correction for a simple crater:

$$x_{slc} = x_a + 0.25 x_a = 1.25 x_a. \tag{14}$$

Combining equations (13) and (14) gives the following overall correction:

$$1.25 x_a = x_{obs} - 0.25 x_a \tag{15}$$

$$1.5 x_a = x_{obs} \tag{16}$$

$$x_a = 0.667 x_{obs}. \tag{17}$$

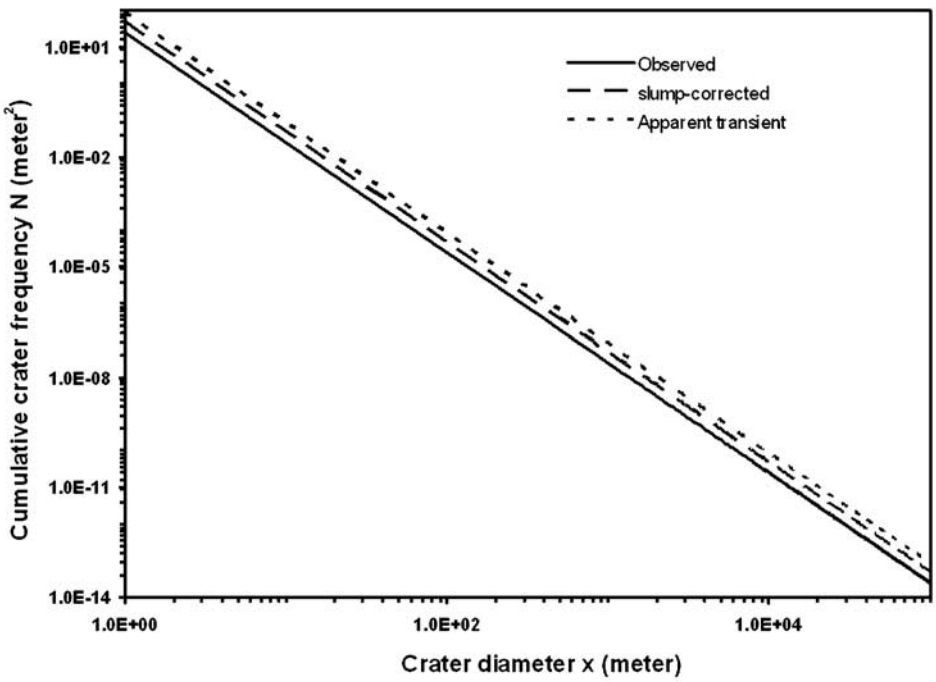

Figure 3. Change of cumulative crater frequency after applying rim and slumping corrections to observed diameter. This plot is for the curve $\gamma = 3$ in Figure 2 after corrections.

[23] The overall correction by equation (17) results in the "apparent" transient crater diameter 33.3% smaller than the finally observed rim-rim diameter. The two corrections resulted in elevated crater size frequencies. Figure 3 shows a plot for the curve with $\gamma = 3$ in Figure 2 after the diameter corrections for the slumping and reference dimension.

4. Stable Program

[24] Since the probability density functions $p(z)$ in equation (2) and $p_r(z)$ in equation (8) can be explicitly solved for only a few cases [*Zolotarev*, 1986], we chose the numerical program STABLE to compute the probability density distributions. STABLE was developed in the Mathematics/Statistics Department, American University for computing the density (PDF), cumulative distribution (CDF), and quantiles for a general stable distribution (J. P. Nolan, Users guide for STABLE 3.04, 2002 (available at http://academic2.american.edu/~jpnolan)). *Nolan* [1999] reported that the STABLE program has a relative accuracy of 10^{-6}. The core of STABLE includes several FORTRAN routines to calculate the probability and distribution functions of standardized densities [*Nolan*, 1999]. The program then used a three-dimensional spline interpolation of the standardized density table to approximate a general stable density function. The routines were based on the formulas presented by *Nolan* [1997]. Before applying the program STABLE, we tested the validity and accuracy of the program STABLE. Because a Gaussian distribution is a special stable distribution, we used STABLE program to generate a Gaussian distribution by providing a set of parameters, and the result showed that the Gaussian distribution can be reproduced accurately. Similar test was done with Cauchy distribution function and the result still holds. As shown in Appendix A, stable distributions are described by four parameters characterizing stability, skewness, scale and shift of the density function [*Nolan*, 1997]. In equation (5), the stability is measured by α, the skewness is 1, the scale by $\lambda^{1/\alpha}$, and the shift is 0. For our purpose, STABLE produced regolith thickness distributions given α and λ.

5. Results

[25] The results of this study were evaluated by two criteria: (1) whether the predicted TAE is consistent with the estimates made previously for Apollo landing sites, and (2) whether the model produces an exotic component constituting 20 to 30% of the lunar soil from distances of 100 km or more.

[26] Previous estimates of regolith thickness from morphologies and seismic experiments at Apollo landing sites are listed in Table 3. All sites except Apollo 12 belong to the upper Imbrian series (UISM) in age. Therefore the regolith thickness observed at the Apollo sites and estimated from the model for UISM are comparable. The derived slopes for the crater size frequency distributions at the Apollo 11 landing site conform to the shallow slope regime, and those at the Apollo 15 and Apollo 17 sites conform to the steep slope regime [*Shoemaker et al.*, 1970; *Neukum et al.*, 1975]. The proposed models are invalid for the Apollo 14 and Apollo 16 landing sites. The derived slopes for the crater size frequency distributions at these two stations are less than $2 + 2h/k$, indicating a violation of the premise of the model (i.e., $\gamma > 2 + 2\ h/k$). The regolith thickness at the Apollo 12 landing site should be close to our estimates for upper Imbrian series mare since the age of Apollo 12 site is

Table 4. Exponents for Crater Ejecta Decay (k), Size Frequency (γ), and Calculated Regolith Thickness

	Upper Imbrium Series Mare		Copernican Mare	
γ	Regolith Thickness 1	Regolith Thickness 2	Regolith Thickness 1	Regolith Thickness 2
		k = 2.5		
2.81	68.5	129.0	15.5	29.2
2.84	14.3	26.5	3.5	6.4
2.88	10.7	19.5	2.7	5.0
2.92	11.7	20.9	3.2	5.6
2.95	17.8	31.3	5.0	8.9
2.99	94.9	129.9	22.2	38.5
		k = 2.61		
2.77	186.3	358.9	39.0	75.2
2.82	9.6	18.0	2.2	4.1
2.86	6.8	12.5	1.7	3.1
2.91	7.7	13.8	2.0	3.7
2.95	12.8	22.6	3.6	6.4
2.99	60.8	105.5	18.0	31.3
		k = 3.0		
2.67	131.9	272.8	21.9	45.2
2.74	2.6	5.1	0.5	1.0
2.80	2.0	3.8	0.5	0.9
2.86	2.6	4.7	0.6	1.2
2.93	5.0	8.8	1.4	2.4
2.99	36.4	63.2	10.8	18.7

dated about 3.16 Ga in age, which lies near the base of the Eratosthenian System [*Wilhelms*, 1987].

5.1. Regolith Thickness

[27] The calculated regolith thicknesses or TAE for the range of conditions we examined in this study are shown in Table 4 and Figure 4. These estimates were made on the basis of the number of craters with diameters one kilometer or larger for upper Imbrian series mare and Copernican mare, and for each of these series. Two types of values for TAE were estimated, TAE (1) (Figures 4a and 4c) for a crater population with the rim to rim diameter correction (equation (12) and TAE (2)) (Figures 4b and 4d) for postslump diameter correction (equation (13)). All estimates were made by using equations (5) and (6) for the shallow slope regime defined by the conditions $2 + 2\,h/k < \gamma < 2 + h$, $\alpha = (\gamma - 2)/h < 1$. Except for the singularity at $\gamma \to 2 + h = 3$ and $\gamma \to 2 + 2\,h/k$, the estimated TAE is generally reasonable. The TAE ranges from 2.0 to 20 m for upper Imbrian series mare, 0.5 to 10 m for Copernican mare. TAE (1), in Figures 4a and 4c, is half the thickness of TAE (2) in Figures 4b and 4d. This is due to the fact that the number of the craters after the correction for the slumping only is smaller than that after the correction to reference dimension as shown in Figure 3. The TAE (2) is an estimate of the maximum, and the most probable values for regolith thickness should fall between TAE (1) and (2).

[28] Figure 4 shows that the TAE is a nonlinear function of γ. Given a specified k value, the TAE begins as large value at the smallest γ, decreases in value at middle range of γ, and then increases as γ increases. This sensitivity is due to the exponential relationship of α to $\lambda^{1/\alpha}$, as $\alpha = (\gamma - 2)/h < 1$ in equation (6). The fact that $\lambda^{1/\alpha}$ is related to time (t) through $C = Fx_0^{\gamma}$ implies that the TAE scales with $t^{1/\alpha}$ if a constant cratering rate is assumed. This indicates that the increase of the TAE is faster than the increasing age of the surface and that large craters dominate the production of new regolith fragments with an increasing surface age.

[29] For the steep slope regime defined by the conditions $\gamma > 2 + h$, and $\alpha = (\gamma - 2)/h > 1$, the estimate of the TAE from equation (7) is sensitive to the smallest crater diameter (x_0) as shown in Figure 5. The smallest TAE ranges from 7.5 to 14 m for upper Imbrian series mare (Figure 5a) and 2.24 to 4.48 m for Copernican mare (Figure 5c) when the specified diameter is one meter. However the smallest TAE is insignificant if a 10-m diameter is used (Figures 5b and 5d). This difference results because fewer craters were included when the larger diameter was used. Comparing the calculated regolith thickness (i.e., TAE) in Table 4 with previous observations at the Apollo 15 and Apollo 17 sites (Table 3) indicates that using one meter resulted in an estimate of regolith thickness comparable to the upper limit of previous observation at Apollo 17, but far exceeds the regolith thickness at the Apollo 15 landing site. There are three reasons for this difference. First, one meter is a small value so that the regolith thickness at the Apollo 17 site was slightly overestimated; second, using a single value for the regolith thickness at the Apollo 15 site (i.e., 5 or 4.4 m in Table 4) poorly represented the distribution of regolith thickness. Lastly, the estimated regolith thickness is inappropriate, and this point will be discussed in next section.

5.2. Lateral Mixing Efficiency

[30] Lateral mixing efficiency indicates whether exotic components constituting 20 to 30% of mare soils can be delivered to a site over distances of 100 km or more. Equation (11) demonstrates that lateral mixing efficiency depends on the three parameters: γ, h, and k. Given $h = 1$, we can derive the values for γ and k required for the

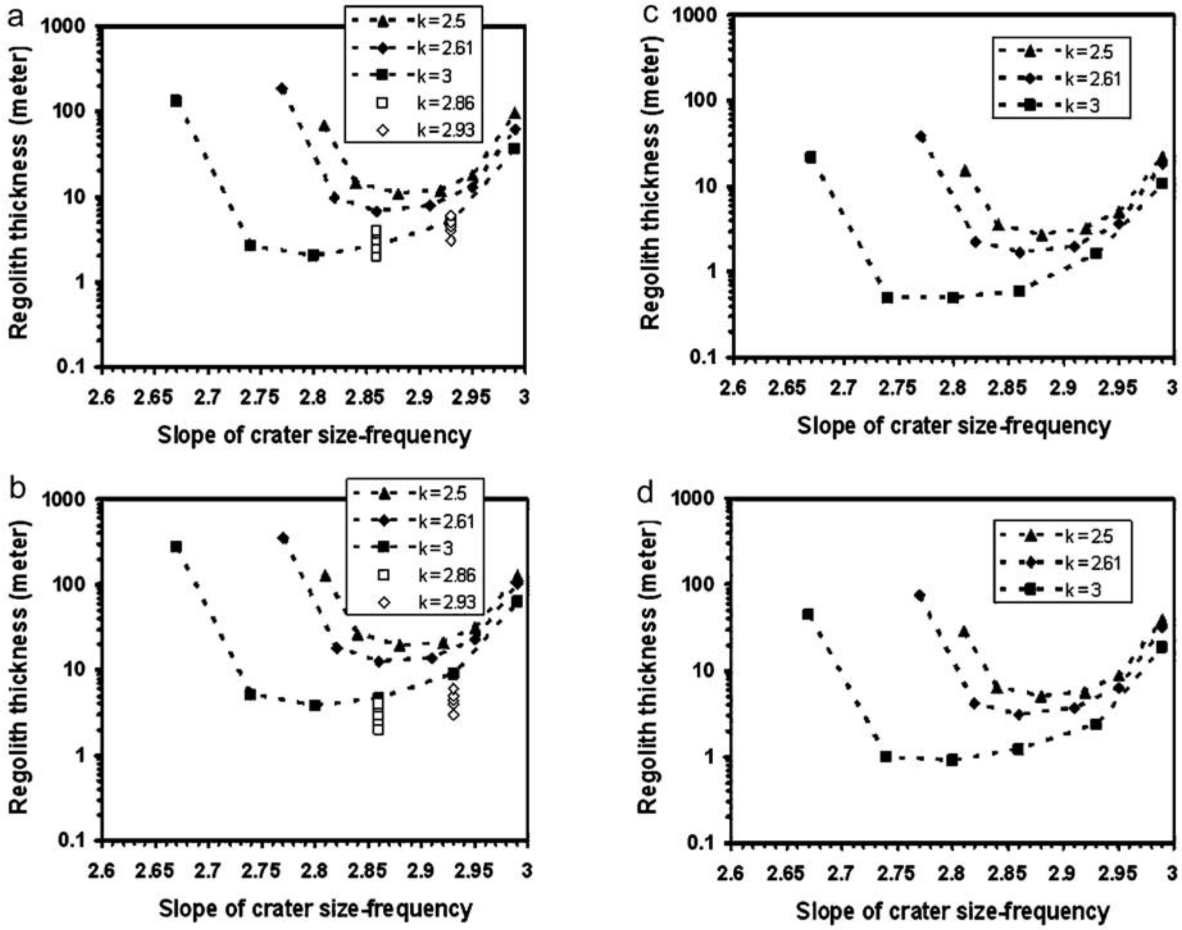

Figure 4. Predicted regolith thickness in shallow slope regime ($2 + 2h/k < \gamma < 2 + h$) for (a, b) upper Imbrian series mare and (c, d) Copernican mare. Figures 4a and 4c show rim diameter correction, and Figures 4b and 4d show postimpact slumping correction. Diamonds represent the estimates of regolith thickness for Apollo 11 in Table 4, and squares represent estimates for Apollo 12.

significant lateral mixing. Substituting 20% for $Z_r(r)$ and 10^5 m for r, we have

$$20\% = 10^{5\varepsilon}. \tag{18}$$

Solving equation (18) results in $\varepsilon = -0.14$. Since

$$\varepsilon = -(k - 2/a_r), \tag{19}$$

where $a_r = \frac{\gamma}{h+k} = \frac{\gamma}{1+k}$, and substituting $\varepsilon = -0.14$ into equation (19) results in

$$\gamma = \frac{2+2k}{k-0.14}. \tag{20}$$

From equation (20), we derive $\gamma = 2.97$ for $k = 2.5$, $\gamma = 2.92$ for $k = 2.61$ and $\gamma = 2.80$ for $k = 3$. By repeating the equivalent steps for $Z_r(r) = 10\%$ and $Z_r(r) = 30\%$, we obtained $\varepsilon = -0.2$ and $\varepsilon = -0.104$. The results are summarized in Table 5.

[31] The dependence of γ on k in equation (20) is plotted in Figure 6. From Figure 6, we can observe that the significant lateral mixing could occur given small values of k and γ, and large craters dominate the formation of fresh regolith by producing large volumes of fresh rock fragments. This follows because craters in this diameter range do not reach an equilibrium state, the slope for such craters in the size frequency plot ranges from 2 to 3. Therefore lateral mixing by craters of this size fits the shallow regime of the proposed model. The results summarized in Table 5 support the conclusion that significant contamination of mare soils by exotic components from beyond the critical distance is possible.

[32] We can apply equation (11) to predict lateral mixing efficiency in the steep slope regime because equation (10) is still valid when $2 + 2\,h/k < \gamma < k + h$. On the basis of the parameter values provided by *Arvidson et al.* [1975], that is, $\gamma = 3.4$, $k = 3$ and $h = 0.94$), we derived equation (21):

$$Z_r(r) = r^{-0.68}. \tag{21}$$

[33] As shown in Figure 7, equation (21) implies even lower lateral mixing efficiency than previous models by *Arvidson et al.* [1975]. Thus our results summarized in Table 5 also indicate that the significant lateral mixing over the critical distance cannot occur in this regime, which is consistent with previous predictions [*Arvidson et al.*, 1975].

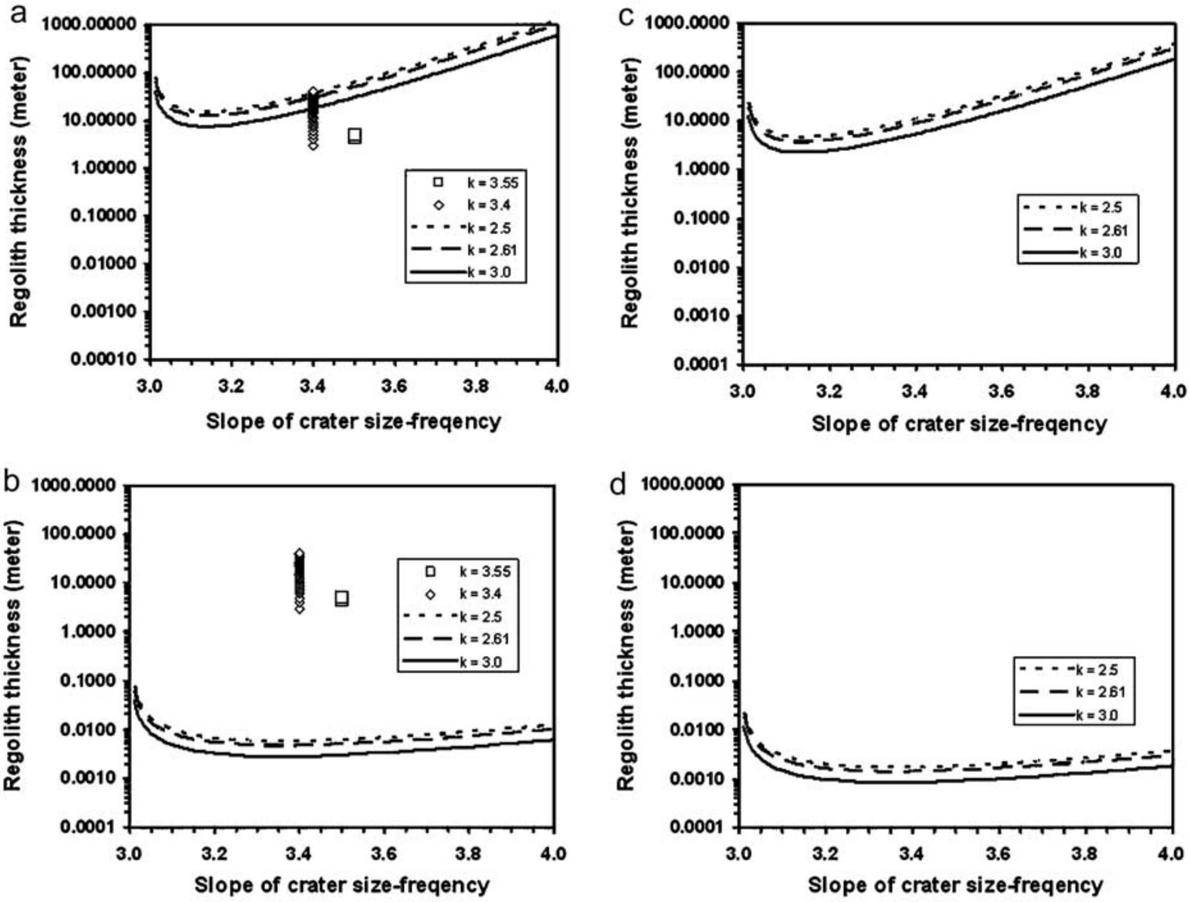

Figure 5. Predicted regolith thickness in steep slope regime ($\gamma > 2 + h$) for (a, b) upper Imbrian Series mare and (c, d) Copernican mare. In Figures 5a and 5c, 1 m is used as the smallest crater diameter, and in Figures 5b and 5d, 10 m is used. Squares represent the estimates of regolith thickness for Apollo 15 in Table 4, and diamonds represent estimates for Apollo 17.

[34] Finally we applied the model to three landing sites Apollo 11, 12 and Luna 24 to test how the model prediction is consistent with geochemical observations. The distances from the nearest highland sites approximate 50 km for Apollo 11, 25 km for Apollo 12, and 40 km for Luna 24 (R. L. Korotev, 2005, personal communication), the slopes for crater size frequency plots are −2.93, −2.86 and −3.0 [*Shoemaker et al.*, 1970; *Boyce et al.*, 1977] and the estimates of highland contamination are 28%, 46% and 10%, respectively [*Korotev and Gillis*, 2001; R. L. Korotev, 2005, personal communication]. Given these distances and an exponent 2.61 for ejecta thickness decay law, the model predicts 19.73% nonmare materials for Apollo 11 site, which is comparable to 28%; 42.11% nonmare materials for Apollo 12, which is close to 46%; and 11.96% nonmare materials for Luna 24 which is very close to 10%. This test further strengthens the conclusion that lateral mixing in the shallow regime is more significant (Apollo 11 and 12) than the steep regime (Luna 24).

6. Discussion

[35] The proposed new model demonstrates that the significant lateral mixing occurs in the shallow slope regime rather than the steep slope regime. Inefficient lateral mixing was suggested by *Arvidson et al.* [1975] using a steep slope for the size frequency distribution of craters. In the discussion below, we first explain why both our model and *Arvidson et al.*'s [1975] predict inefficient lateral mixing in the steep slope regime, and then address why mare soils have approximately higher (∼20%) highland contamination while highland soils have much lower mare contamination [*Hörz*, 1978; *Korotev*, 1997; *Ziegler et al.*, 2003, 2004].

6.1. Lateral Mixing in the Shallow Slope Regime

[36] First, both models use the mean of the regolith thickness in predicting lateral mixing efficiency. *Housen et al.* [1979] suggested that regolith thickness should be estimated in terms of a surface probability distribution and

Table 5. Slopes (γ) of Crater Size Frequency for Transporting a Percentage of Exotic Component

k	10% Exotic	20% Exotic	30% Exotic
2.5	3.043	2.97	2.92
2.61	2.995	2.92	2.88
3.0	2.85	2.80	2.76

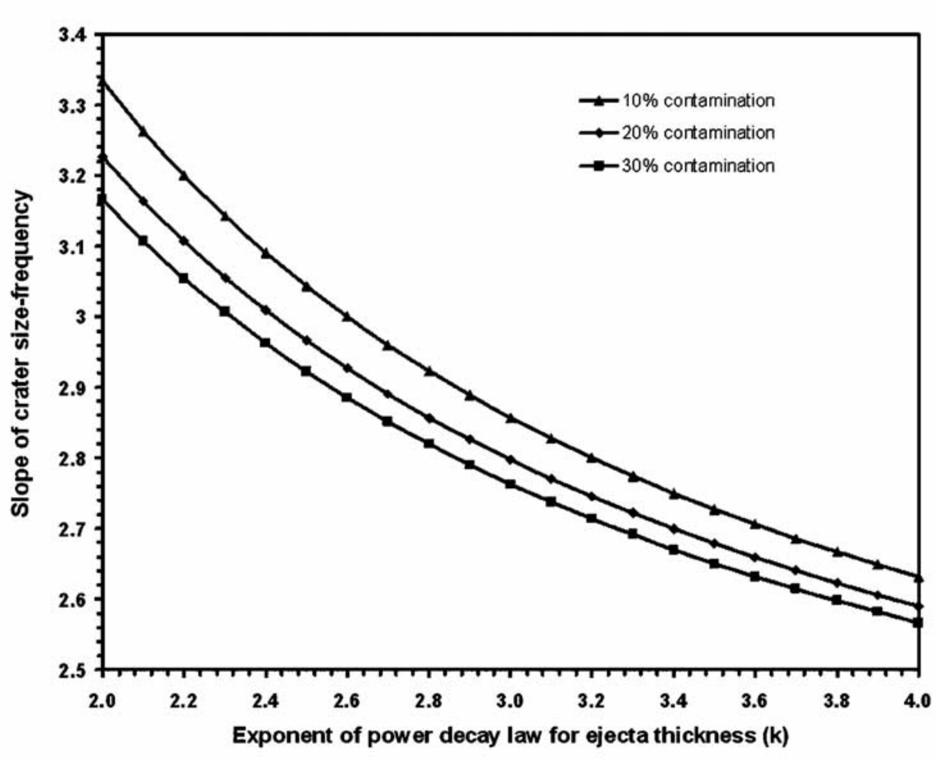

Figure 6. Variation of the slopes (γ) of the crater size frequency with the exponent (k) of ejecta decay law given the percentage of material contamination. These relationships are based on equation (17) and parameter values listed in Table 5.

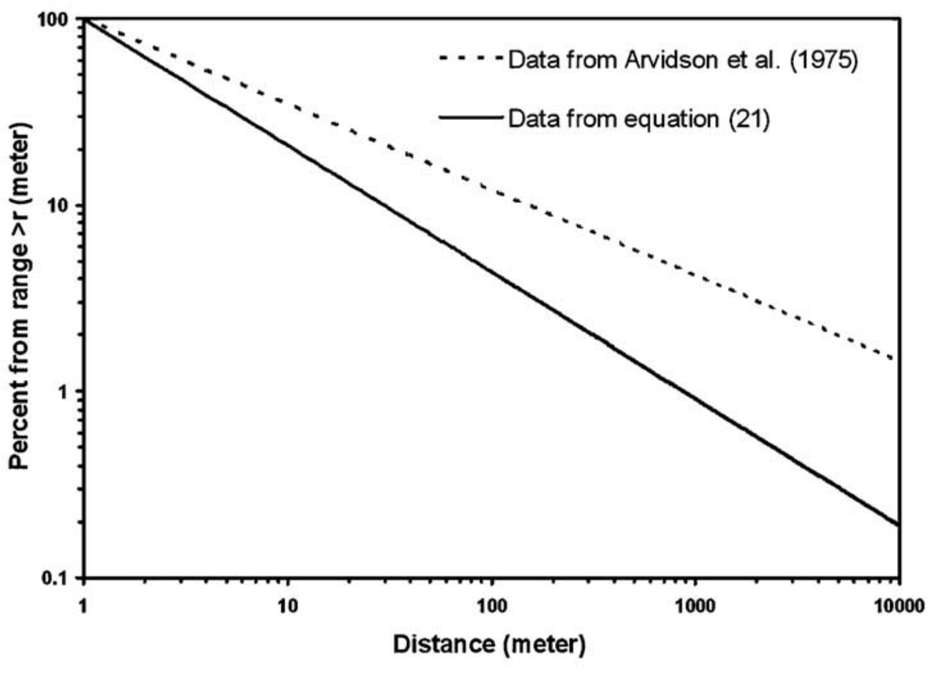

Figure 7. Range frequency distributions for the exotic components laterally transported over distances exceeding 1 m in the steep slope regime. The distributions are defined by the relationship $Z_r(r) = r^{\varepsilon}$, and $\varepsilon = -0.46$ and -0.68.

treated as a function of the fraction of the surface over which they apply. As such, the mode of the density function for regolith thickness distribution rather than an average should be used as a representative value of regolith thickness for a given area. In the steep slope regime, the probability distribution of regolith thickness might be expected to have a representative thickness (i.e., the mode) corresponding to a surface dominated by many small craters because they occupy more surface area than large ones do. However, the values for the regolith thickness are confounded by the significant probability of large impact crater mixing. It is very common that one just use the average lunar regolith as reference when discussing the contamination of exotic material into lunar regolith, ignoring the fact that lunar regolith is not homogeneous in thickness and exhibits a probability distribution. An estimated average thickness from the full spectrum of craters diameters would likely represent regolith thickness formed by neither many small or large craters.

[37] Second, reexamining the assumption in both models indicates that neither could accommodate the shielding effects on regolith growth, especially efficient in the steep slope regime. In the early development of regolith, a full spectrum of craters sizes contributed to regolith production and the shielding effect on regolith growth from small craters was insignificant because regolith was relatively thin. This assumption of linear addition is likely valid because crater ejecta have not saturated the surface [*Housen et al.*, 1979]. However, the shielding effect of regolith becomes significant as the regolith thickens, increasing the number of small craters "filtered" out [*Lindsay*, 1975; *Quaide and Oberbeck*, 1975; *Housen et al.*, 1979]. Small craters (<100 m) form mainly within the regolith and do not contribute to modifying the regolith growth. Instead, they churn the regolith, dispersing it laterally. Their impacts are shallow leaving small craters containing much larger volumes of reworked regolith [*Shoemaker et al.*, 1970; *Gault et al.*, 1974]. Therefore the assumption of linear addition is invalid for a lateral mixing model in the steep regime and should be modified to accommodate multiple movements of the regolith grains [*Li and Mustard*, 2000].

[38] We have argued that lateral mixing in the shallow slope regime is able to produce significant lateral mixing from beyond the critical distance. This contradicts previous determinations of only 5% abundance of exotic component at distances of 30 km away from mare and highland contacts [*Li and Mustard*, 2000]. It also brings into question how well remotely sensed data can resolve the compositional gradient across mare-highland contact [*Quaide and Oberbeck*, 1975]. Our previous observations of lateral mixing were focused on specific boundaries or regions, and the end-members for spectral mixture analysis were chosen from these specific regions [*Li and Mustard*, 2000]. It is possible that the selected end-members were contaminated and the observed fractions might be biased or underestimated. Additionally, optical remote sensing is only able to penetrate a few mm of the regolith surface. This depth is right on the top of reworked zones where regolith mixing is dominated by small craters [*Gault et al.*, 1974; *Quaide and Oberbeck*, 1975]. Below this reworked zone, depositional units of various thicknesses produced by relatively small craters may be found because the reworking and gardening of small craters is inefficient in vertically mixing all regolith layers. The appropriate use of the presented model within the shallow slope regime is for surfaces mostly occupied by unsaturated craters. It is also applicable for estimating the exotic component within the regolith layers below the reworked zone (P. H. Schultz, 2002, personal communication). We therefore believe that the significant material contamination could occur beyond the critical distance below the reworked zone.

6.2. Why More Highland Contamination in Mare Than Mare in Highland Region?

[39] One dilemma with efficient lateral mixing on the Moon is how to explain more highland contamination in the mare than mare contamination in the highlands. Mass balance constraints suggest that only 6% of the Apollo 16 regolith derives from the maria, which is far less than highland contamination in mare region [*Hörz*, 1978; *Korotev*, 1997; *Ziegler et al.*, 2003, 2004]. If the majority of contamination comes from lateral mixing, rather than vertical, then shouldn't the highland value be the same as the mare one (B. Bussey, 2004, personal communication)?

[40] While our current model cannot be used to address this issue, here we give our interpretation to this dilemma and highlight several factors that should be considered in future modeling. First, mare accounts for only 17% lunar surface area, while highland accounts for the remaining 83% lunar surface. If a spatially uniform distribution of craters is assumed, the total number of craters in the mare is much fewer than in the highland. Naturally it is expected that there are more craters in the highland contributing to the delivery of more highland materials to mare region than in the opposite direction. Integrative effects would be that a larger amount of highland must have been transported into mare region than vise versa per unit area. Second, relatively large craters are random in location but far from spatially uniform because they have a tendency to be found in the highland because of the larger highland surface area than mare. If large craters play a significant role during lateral mixing as shown by *Li and Mustard* [2003], then more highland contamination to mare soils should be expected. Third, the limitation to the availability of contaminating source materials must be considered in a model, and this will take into account the effects of the different surface area of both mare and highland on lateral mixing. In this sense, a sophisticated numerical model should be developed.

7. Conclusions

[41] A mathematical model is proposed for estimating lateral mixing efficiencies on the Moon. Two regimes divided lateral mixing by the shallow slope and steep slope of crater size frequency distribution. The model predicts that in the shallow slope regime, typical regolith thickness ranges from 2.0 to 20 m for upper Imbrian series mare and 0.5 to 10 m for Copernican mare. If we assume a constant cratering rate and the shallow slope regime, the increase of the regolith thickness is faster than the increasing age of the surface, and a nonlinear increase of regolith thickness produced by large craters.

[42] This study indicates that lateral mixing in the shallow slope regime can deliver a significant amount (20 to 30%)

of the exotic material over distances 100 km or larger, while the steep slope regime cannot. The prediction of inefficient lateral mixing in the steep slope regime results from failing to accommodate the shielding effect of regolith on small craters. The assumption of linear addition of the regolith in this regime is likely not valid. This explains why the models both presented here and by *Arvidson et al.* [1975] predicted very low lateral mixing efficiency. A model for dealing with lateral mixing in the steep slope regime should account for this shielding effect.

[43] Since optical remote sensing penetrates only a few mm of regolith surface well within the reworked zone, we would expect depositional units of various thicknesses to be hidden by the reworked zone of small craters. Our model under the shallow slope regime is appropriate for estimating the exotic component of these regolith layers below the reworked zone, though it cannot be confirmed optically, and that significant material contamination could occur over the critical distance.

Appendix A: Stable Probability Distribution

[44] A stable distribution is the name for a family of density distributions that allows skewness and heavy tails [*Nolan*, 1997, 1999]. These distributions were characterized by *Lévy* [1954] in his study of sums of independent identically distributed (IID) terms. The word stable was used to denote invariant shape under sums of IID terms. A mathematically strict definition of a stable distribution can be found in work by *Feller* [1971] and *Zolotarev* [1986]. In a few words, a distribution is stable if a sum of IID variables has the same density distribution as the individual variables in the sum [*Gorenflo and Mainardi*, 1998]. Three well-known probability functions, Gaussian, Cauchy and Lévy distributions, are the specific cases of the stable distribution because these distributions have closed expressional forms for the density. The closed formulas for densities and distribution for all others are not available. The densities and distributions for stable distributions are calculated numerically from their characteristic functions (e.g., equations (5) and (9)).

[45] The characteristic function most commonly used for stable distributions is given by *Samorodnitsky and Taqqu* [1994]:

$$\phi(\mu) = \begin{cases} \exp(-\sigma^{\alpha}|\mu|^{\alpha}[1 - i\beta\mathrm{sgn}(\mu)\tan(\pi\alpha/2)] + it\mu)\} & \alpha \neq 1 \\ \exp\left(-\sigma|\mu|\left[1 + i\beta\frac{2}{\pi}\mathrm{sgn}(\mu)\ln|\mu|\right] + it\mu\right)\} & \alpha = 1, \end{cases} \tag{A1}$$

where $i = [-1]^{0.5}$. One can see a stable distribution is determined by four parameters: an index of stability α, a skewness parameter β, a scalar σ and a location parameter t [*Nolan*, 1997]. The value range of the parameters is $0 < \alpha \leq 2$, $-1 \leq \beta \leq 1$, and $\sigma > 0$. t is any real number. The shape of a stable distribution is determined by α and β. The case of $\alpha = 2$ and $\beta = 0$ defines Gaussian function, while $\alpha = 1$ and $\beta = 0$ defines Cauchy function. Because a stable function allows a heavy tail, hence permits infinite variance, the Cauchy function was used in an anomalous diffusion model for the compositional gradient across mare-highland contacts [*Li and Mustard*, 2000]. In this study, $\alpha < 1$ for the shallow steep regime, $\alpha > 1$ for the steep slope regime, $\beta = 1$, $t = 0$ and $\sigma = \lambda^{1/\alpha}$.

Appendix B: Lateral Mixing Model

[46] First, we will derive equation (2), and evaluate equation (8) by applying equation (3) and (4). Finally, we will present the derivation of $f(x)$ in equation (3). The Cartesian coordinates shown in Figure B1 are used to facilitate the discussion, in which $\boldsymbol{r}$ denotes a vector of the length r. We will derive the probability density distribution of Z, representing the total accumulation of ejecta (TAE) at the origin, and Z_r, representing the total accumulation of ejecta thickness (TAE) beyond outside of a circle $\boldsymbol{r}$.

B1. Derivation of Equation (2)

[47] Our derivation is based on the Markov method [*Chandrasekhar*, 1943] and the assumption of a linear addition of crater ejecta. Given an ejecta thickness distribution ($\zeta(x, \mathrm{r})$) of craters with diameter x, we write TAE resulting from N craters beyond a circle of radius r as

$$Z = \int \zeta(x, \boldsymbol{r}) dN(x, \boldsymbol{r}). \tag{B1}$$

Let r and N approach infinity simultaneously such that

$$\pi r^2 F = N \tag{B2}$$

($r \rightarrow \infty$; $N \rightarrow \infty$; F = constant).
Recall F denotes the total number of craters with diameter $x_0 < x < x_m$ per unit area. The Markov approach results in equation (A3) between the probability density distribution ($p(\boldsymbol{Z})$) and its characteristic function ($\phi_N(u)$),

$$p_N(\boldsymbol{Z}_0) = \frac{1}{4\pi^2} \int_{-\infty}^{\infty} \exp(-i\boldsymbol{u} \cdot \boldsymbol{Z}_0)\phi_N(\boldsymbol{u})d\boldsymbol{u}, \tag{B3}$$

where

$$\phi_N(\boldsymbol{u}) = \prod_{i=1}^{N} \int_{x_0}^{x_m} \int_{r'_i=0}^{r} \exp\left(i\boldsymbol{u} \cdot \zeta_i\left(x_i, \boldsymbol{r}'_i\right)\right) \times f_i\left(x_i, \boldsymbol{r}'_i\right) d\boldsymbol{r}'_i dx_i. \tag{B4}$$

Here f_i (x_i, $\boldsymbol{r}_i'$) denotes the probability of occurrence of the ith crater at the location r_i with a diameter x_i. We now assume that the only fluctuations in Z that are compatible with the average crater density occur, then

$$f_i\left(x_i, \boldsymbol{r}'_i\right) = \frac{1}{\pi r^2} f(x), \tag{B5}$$

where $f(x)$ is the frequency of the craters with different diameters given in equation (3). With equation (B5), equation (B4) becomes

$$\phi_N(\boldsymbol{u}) = \left[\frac{1}{\pi r^2} \int_{x_0}^{x_m} \int_{r'=0}^{r} \exp(i\boldsymbol{u} \cdot \zeta(x, \boldsymbol{r}')) \times f(x) d\boldsymbol{r}' dx\right]^N. \tag{B6}$$

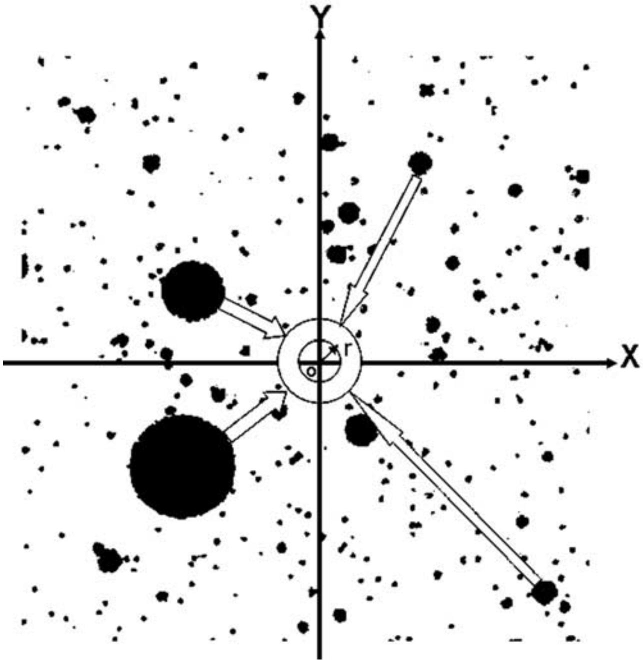

Figure B1. Coordination system for lateral mixing model, from which the total accumulative ejecta thickness is derived both at the origin (o) and from outside of the circle r. Black circles represent randomly distributed craters generated through computer simulation.

[48] We now let r and N tend to infinity according to equation (B2); thus

$$\begin{aligned}\phi(\boldsymbol{u}) &= \lim_{r\to\infty, N\to\infty} \phi_N(\boldsymbol{u}) \\ &= \lim_{r\to\infty, N\to\infty}\left[\frac{1}{\pi \boldsymbol{r}^2}\int_{x=0}^{\infty}\int_{r'=0}^{r} \exp(i\boldsymbol{u}\cdot\zeta(x,\boldsymbol{r}'))\times f(x)d\boldsymbol{r}'dx\right]^{\pi \boldsymbol{r}^2 F}.\end{aligned} \tag{B7}$$

Because

$$\frac{1}{\pi r^2}\int_{x_0}^{x_m}\int_{r'=0}^{r} f(x)dxd\boldsymbol{r}' = 1, \tag{B8}$$

we can then rewrite the expression for $\phi(\boldsymbol{u})$ in the form

$$\begin{aligned}\phi(\boldsymbol{u}) &= \lim_{r\to\infty}\left[1-\frac{1}{\pi r^2}\int_{x_0 0}^{x_m}\int_{r'=0}^{r}[1-\exp(i\boldsymbol{u}\cdot\zeta(x,\boldsymbol{r}'))]\times f(x)d\boldsymbol{r}'dx\right]^{\pi r^2 F} \\ &= \exp\left[F\int_{x_0}^{x_m} p(x)dx\int_0^{\infty}[\exp(i\boldsymbol{u}\zeta(x,r))-1]2\pi r dr\right] \\ &= \exp\left[\int_{x_0}^{x_m}\xi(x)dx\int_0^{\infty}[\exp(i\boldsymbol{u}\zeta(x,r))-1]2\pi r dr\right],\end{aligned} \tag{B9}$$

where $\xi(x) = Ff(x)$.

B2. Evaluation of Equation (9)

[49] Substituting equations (3) and (4) into equation (B9) and replacing zero for the inner integral limit by r, we derive

$$\begin{aligned}\phi_r(\boldsymbol{u}) &= \exp\left[\int_{x_0}^{x_m}\xi(x)dx\int_r^{\infty}[\exp(iu\zeta(x,r))-1]2\pi r dr\right] \\ &= \exp\left\{\int_{x_0}^{x_m}\frac{\gamma F_0 x_0^{\gamma}}{1-(x_0/x_m)^{\gamma}}\frac{1}{x^{\gamma+1}}dx\int_r^{\infty}2\pi r\left[e^{iuR_0x^h\left(\frac{x}{2r}\right)^k}-1\right]dr\right\}.\end{aligned} \tag{B10}$$

With the transformations

$$y = R_0x^h(x/2r)^k,\quad r = \frac{x}{2}\left(\frac{R_0h}{y}\right)^{1/k},\quad \text{and}\quad dr = -\left(\frac{R_0^{1/k}}{2k}\right)\frac{x^{h/k+1}}{y^{1/k+1}}dy$$

equation (B10) is transformed into

$$\begin{aligned}\phi_r(u) &= \exp\left(\int_{x_0}^{x_m}\frac{\pi\gamma F x_0^{\gamma}R_0^{2/k}}{2[1-(x_0/x_m)^{\gamma}]x^{(\gamma-2-2h/k)+1}}dx\int_0^{R_0x^h(x/2r)^k}\frac{(e^{iuy}-1)}{ky^{\frac{2}{k}+1}}dy\right) \\ &= \exp\left(\int_{x_0}^{x_m}\frac{\sigma}{2x^{(\gamma-2-2h/k)+1}}dx\int_0^{R_0x^h(x/2r)^k}\frac{(e^{iuy}-1)}{ky^{\frac{2}{k}+1}}dy\right),\end{aligned} \tag{B11}$$

where $\sigma = \frac{\pi\gamma F x_0^{\gamma}R_0^{2/k}}{[1-(x_0/x_m)^{\gamma}]}$.

Integrating equation (B11), we obtain

$$\begin{aligned}\phi_r(\boldsymbol{u}) &= \exp\left\{\frac{\sigma}{2}\frac{-1}{(\gamma-2-2h/k)x^{\gamma-2-2h/k}}\int_0^{R_0x^h(x/2r)^k}\frac{(e^{iuy}-1)}{ky^{\frac{2}{k}+1}}dy\Bigg|_{x_0}^{x_m}\right. \\ &\quad\left.+\frac{\sigma}{2}\int_{x_0}^{x_m}\frac{R_0(h+k)x^{h-1}(x/2r)^k}{(\gamma-2-2h/k)x^{\gamma-2-2h/k}}\frac{e^{iuR_0x^h(x/2r)^k}-1}{k\left(R_0x^h(x/2r)^k\right)^{1+2/k}}dx\right\} \\ &= \exp\left\{\frac{\sigma}{2}\frac{1}{(\gamma-2-2h/k)x_0^{\gamma-2-2h/k}}\int_0^{R_0x_0^h(x_0/2r)^k}\frac{e^{iuy}-1}{ky^{1+2/k}}dy\right. \\ &\quad-\frac{\sigma}{2}\frac{1}{(\gamma-2-2h/k)x_m^{\gamma-2-2h/k}}\int_{R_0x_0^h(x_0/2r)^k}^{R_0x_m^h(x_m/2r)^k}\frac{e^{iuy}-1}{ky^{1+2/k}}dy \\ &\quad-\frac{\sigma}{2}\frac{1}{(\gamma-2-2h/k)x_m^{\gamma-2-2h/k}}\int_0^{R_0x_0^h(x_0/2r)^k}\frac{e^{iuy}-1}{ky^{1+2/k}}dy \\ &\quad+\frac{\sigma}{2}\frac{R_0^{\left(\frac{\gamma-2}{h}-\frac{2}{k}\right)}}{(\gamma-2-2h/k)(2r)^{k\left(\frac{\gamma-2-2h/k}{k+h}\right)}}\int_{R_0x_0^h(x_0/2r)^k}^{R_0x_m^h(x_m/2r)^k} \\ &\quad\left.\cdot\frac{1}{y^{\left(\frac{\gamma-2-2h/k}{k+h}\right)}}\frac{e^{iuy}-1}{ky^{1+2/k}}dy\right\}.\end{aligned} \tag{B12}$$

[50] For the limit $x_m \rightarrow \infty$, requires $\gamma > 2 + 2\,h/k$, $k > 2$ for the derivation of equation (B13) from equations (B12),

$$\phi_r(\boldsymbol{u}) = \exp\left\{\frac{\sigma}{2}\frac{1}{(\gamma-2-2h/k)x_0^{\gamma-2-2h/k}}\int_0^{R_0x_0^h(x_0/2r)^k}\frac{e^{iuy}-1}{ky^{1+2/k}}dy + \frac{\sigma}{2}\frac{R_0^{\left(\frac{\gamma-2}{h}-\frac{2}{k}\right)}}{k(\gamma-2-2h/k)(2r)^{k\left(\frac{\gamma-2-2h/k}{k+h}\right)}}\int_{R_0x_0^h(x_0/2r)^k}^{R_0x_m^h(x_m/2r)^k}\frac{e^{iuy}-1}{y^{\left(\frac{\gamma}{k+h}+1\right)}}dy\right\}. \tag{B13}$$

[51] For the limit $x_0 \rightarrow 0$, we require $\gamma < k + h$. Equation (9) can be obtained by evaluating the second integral of equation (B13) [*Gnedenko and Kolmogorov*, 1954].

B3. Derivation of *f*(*x*) in Equation (3)

[52] It is known that the crater size frequency on the Moon obeys a power law. Let x denote a crater diameter, then we can write the crater number with diameters > x in unit area $N = kx^{-\gamma}$, where k and γ are constant. $N = F$ for $x = x_0$ and $N = 0$ for $x_m = \infty$. The total number of craters with diameter ranging from x_0 to x_m,

$$F' = kx_0^{\gamma} - kx_m^{\gamma}. \tag{B14}$$

[53] We can derive the number of craters with diameters from x to $x + dx$ by differentiating N,

$$\frac{dN}{dx} = -\gamma k x^{-\gamma-1}. \tag{B15}$$

Finally, dividing equation (B15) by equation (B14) gives us $f(x)$ in equation (3), the probability density of crater with diameter x.

Notation

$dN(x, \boldsymbol{r})$	number of craters of diameter x to x + dx in a small region d$\mathbf{r}$ centered on point $\boldsymbol{r}$.
x	crater diameter in meters.
$\boldsymbol{r}$	vector representing crater location.
Z	total accumulative ejecta thickness.
$\zeta(x, r)$	blanket thickness of a crater having diameter x at location $\boldsymbol{r}$.
$\xi(x)$	expected number of craters of diameter x, per unit area per unit diameter interval.
$p(z)$	probability density function of Z.
$\phi(Z)$	characteristic function (CF) of $p(Z)$.
x_m	maximum crater diameters.
x_0	minimum crater diameters.
F	total number of craters per unit area (m^2) with diameter $x_0 < x < x_m$.
C	constant.
$f(x)$	percentage frequency of craters with a diameter x in total crater population.
γ	exponent of the power law describing the crater size frequency distribution.
R_0x^h	ejecta thickness at the crater rim.
R_0	coefficient.
h	exponent of the power law describing ejecta thickness at the crater rim.
k	exponent of the power law describing ejecta thickness decay as a function of r.
$\Gamma(\cdot)$	Gamma function.
$\alpha = (\gamma - 2)/h$	exponent in $\phi(u)$.
$E[Z]$	mean value of total accumulation of ejecta thickness Z.
$p_r(z)$	probability density function of Z carrying from beyond a circle centered at the origin and having a diameter r.
$\phi_r(u)$	characteristic function of $p_r(z)$.
$\alpha_r = (\gamma + k)/h$	exponent in $\phi_r(u)$.
Z_r	range frequency function.
$\varepsilon = -(k - 2/\alpha_r)$	exponent in range frequency function.
X_{obs}	observed crater diameter.
X_{slc}	slump-corrected crater diameter.
x_a	"apparent" transient crater diameter.

[54] **Acknowledgments.** This work has greatly benefited from many discussions with Peter H. Schultz, Tao Pang, and Xia Ma. We would like to thank Michael Whiting, whose contributions improved the quality of the manuscript. We thank R. Korotev, B. Bussey, C. Chapman, and an anonymous reviewer for their helpful comments. R. Korotev kindly provided several examples for testing the model. This work would not have been possible without the code of John P. Nolan and technical support from Lynn Carlson and Bill Fripp. Thanks are extended to the NASA Planetary Geology and Geophysics Program for supporting this study.

References

Adler, I., M. Podwysocki, C. Andre, J. Trombka, E. Eller, R. Schmadebeck, and L. Yin (1974), The role of horizontal transport as evaluated from the Apollo 15 and 16 orbital experiments, *Proc. Lunar Sci. Conf. 5th*, 975–979.

Arnold, J. R. (1975), Monte Carlo simulation of turnover processes in the lunar regolith, *Proc. Lunar Sci. Conf. 6th*, 2375–2395.

Arvidson, R. E., R. O. Drozd, C. M. Hohenberg, C. J. Morgan, and G. Poupeau (1975), Horizontal transport of the regolith, modification of features, and erosion rates on the lunar surface, *Moon*, *13*, 67–79.

Baldwin, R. B. (1985), Relative and absolute ages of individual craters and the rate of infalls on the Moon in the post-Imbrium period, *Icarus*, *61*, 63–91.

Blewett, D. T., B. R. Hawke, P. G. Lucey, G. J. Taylor, R. Jaumann, and P. D. Spudis (1995), Remote sensing and geologic studies of the Schiller-Schickard region of the Moon, *J. Geophys. Res.*, *100*, 16,959–16,977.

Boyce, J. M., G. G. Schaber, and A. L. Dial (1977), Age of Luna 24 mare basalts based on crater studies, *Nature*, *265*, 38–39.

Campbell, B. A., J. B. Bell III, S. H. Zisk, B. R. Hawke, and K. Horton (1992), A high-resolution radar and CCD imaging study of crater rays in mare Serenetatis and mare Nectaris, in *Proc. Lunar Planet. Sci. Conf. 22nd*, 259–274.

Chandrasekhar, S. (1943), Stochastic problems in physics and astronomy, *Rev. Mod. Phys.*, *15*, 1–87.

Chapman, C., and W. B. McKinnon (1986), Cratering of planetary satellites, in *Satellites*, edited by J. A. Burns and M. S. Mathews, pp. 492–580, Univ. of Ariz. Press, Tucson.

Evensen, N. M., V. R. Murthy, and M. R. Coscio (1974), Provenance of KREEP and the exotic component: Elemental and isotopic studies of grain size fraction in lunar soils, *Proc. Lunar Planet. Sci. Conf. 5th*, 1401–1417.

Farrand, W. H. (1988), Highland contamination and minimum basalt thickness in northern Mare Fecunditatis, *Proc. Lunar Planet. Sci. Conf. 18th*, 319–329.

Feller, W. (1971), *An Introduction to Probability Theory and its Applications*, vol. 2, 2nd ed., John Wiley, Hoboken, N. J.

Fischer, E. M., and C. M. Pieters (1995), Lunar surface aluminum and iron concentration from Galileo solid state imaging data, and the mixing of mare and highland materials, *J. Geophys. Res.*, *100*, 23,279–23,290.

Florenskiy, K. P., A. T. Bazilevskiy, and V. A Ivanov (1974), The role of exogenic factors in the formation of the lunar surface, in *Proceedings of the Soviet-American Conference on Cosmochemistry of the Moon and Planets*, edited by J. H. Pomerov and N. H. Hubbard, pp. 571–584, NASA, Washington, D. C.

Gault, D. E., F. Hörz, D. E. Brownlee, and J. B. Hartung (1974), Mixing of the lunar regolith, *Proc. Lunar Sci. Conf. 5th*, 2365–2386.

Gnedenko, B. V., and A. N. Kolmogorov (1954), *Limit Distribution for Sums of Independent Random Variables*, pp. 164–171, Addison-Wesley, Boston, Mass.

Gorenflo, R., and F. Mainardi (1998), Random walk models for space-fractional diffusion processes, *Fractional Calculus Appl. Anal.*, *1*, 1677–1691.

Hawke, B. R., D. T. Blewett, P. G. Lucey, G. A. Smith, J. F. Bell III, B. A. Cambell, and M. S. Robinson (2004), The origin of lunar crater rays, *Icarus*, *170*, 1–16.

Head, J. W., S. Murchie, J. F. Mustard, C. M. Pieters, G. Neukum, A. McEwen, R. Greeley, E. Nagel, and M. J. S. Belton (1993), Lunar impact basins: New data for the western limb and far side (Orientale and South Pole-Aitken basins) from the first Galileo flyby, *J. Geophys. Res.*, *98*, 17,149–17,181.

Hörz, F. (1978), How thick are mare basalts?, *Proc. Lunar Planet. Sci. Conf. 9th*, 3311–3331.

Hörz, F., R. Grieve, G. Heiken, S. Spudis, and A. Binder (1991), Lunar surface processes, in *Lunar Sourcebook*, edited by G. Heiken, D. Vaniman, and B. M. French, pp. 61–120, Cambridge Univ. Press, New York.

Housen, K. R., L. Wilkening, C. Chapman, and R. Greenberg (1979), Regolith development and evolution of asteroids and the Moon, in *Asteroids*, edited by T. Gehrels, pp. 601–627, Univ. of Ariz. Press, Tucson.

Housen, K. R., R. M. Schmidt, and K. A. Holsapple (1983), Crater ejecta scaling laws: Fundamental forms based on dimensional analysis, *J. Geophys. Res.*, *88*, 2485–2499.

Jolliff, B. L., J. J. Gillis, R. L. Korotev, and L. A. Haskin (2000), On the origin of nonmare materials at the Apollo 12 landing site, *Lunar Planet. Sci.* [CD-ROM], *XXXI*, abstract 1671.

Korotev, R. L. (1997), Some things we can infer about the Moon from the composition of the Apollo 16 regolith, *Meteorit. Planet. Sci.*, *32*, 447–478.

Korotev, R. L., and J. J. Gillis (2001), A new look at the Apollo regolith and KREEP, *J. Geophys. Res.*, *106*, 12,339–12,353.

Korotev, R. L., B. L. Jolliff, and R. Z. Ziegler (2000), The KREEP components of the Apollo 12 regolith, *Lunar Planet. Sci.* [CD-ROM], *XXXI*, abstract 1363.

Laul, J. C., and J. J. Papike (1980), The lunar regolith: Comparative chemistry of the Apollo sites, *Proc. Lunar Planet. Sci. Conf. 11th*, 1307–1340.

Laul, J. C., J. J. Papike, and S. B. Simon (1981), The lunar regolith: Comparative studies of the Apollo and Luna sites: Chemistry of soils from Apollo 17, Luna 16, 20 and 24, *Proc. Lunar Planet. Sci. Conf., 12th, Ser. B*, 389–407.

Lévy, P. (1954), *Theorie de l'Addition des Variables Aleatoires*, 2nd ed., Elsevier, New York.

Li, L., and J. F. Mustard (2000), Compositional gradients across mare-highland contacts: The importance of lateral mixing and geological implications, *J. Geophys. Res.*, *105*, 20,431–20,450.

Li, L., and J. F. Mustard (2003), Highland contamination in lunar mare soils: Improved mapping with multiple end-member spectral mixture analysis (MESMA), *J. Geophys. Res.*, *108*(E6), 5053, doi:10.1029/2002JE001917.

Lindsay, J. J. (1975), A steady-state model for the lunar soil, *Geol. Soc. Am. Bull.*, *86*, 1661–1670.

Marcus, A. H. (1969), On vector fields generated by 'moving average' of a random points process, *John Hopkins Dep. Stat. Tech. Rep. 103*, Johns Hopkins Univ., Baltimore, Md.

Marcus, A. H. (1970), Distribution and covariance function of elevations on a cratered planetary surface, *Moon*, *1*, 297–337.

McGetchin, T. R., M. Settle, and J. W. Head (1973), Radial thickness variation in impact crater ejecta: Implications for lunar basins deposits, *Earth Planet. Sci. Lett.*, *20*, 226–236.

McGill, G. E. (1977), Craters as "fossils": The remote dating of planetary surface materials, *Geol. Soc. Am. Bull.*, *88*, 1102–1110.

Melosh, H. J. (1980), Cratering mechanics-observational, experimental and theoretical, *Annu. Rev. Earth Planet. Sci.*, *8*, 65–93.

Murthy, V. R. (1975), The source and origin of the exotic component and KREEP-rich materials on the Moon, *Moon*, *13*, 111–119.

Mustard, J. F., and J. W. Head (1996), Buried stratigraphic relationships along the southwestern shores of Oceanus Procellarum: Implications for early lunar volcanism, *J. Geophys. Res.*, *101*, 18,913–18,925.

Mustard, J. F., L. Li, and G. He (1998), Nonlinear spectral mixture modeling of lunar multispectral data: Implications for lateral transport, *J. Geophys. Res.*, *103*, 19,419–19,425.

Nakamura, Y., J. Dorman, F. Duennebier, D. Lammlein, and G. Latham (1975), Shallow lunar structure determined from the passive seismic experiment, *Moon*, *13*, 57–66.

Neukum, G., B. Konig, H. Fechtig, and D. Storzer (1975), Cratering in the Earth-Moon system: Consequences for age determination by cratering counting, *Proc. Lunar Sci. Conf. 6th*, 2597–2620.

Nolan, J. P. (1997), Numerical calculation of stable densities and distribution function, *Stochastic Models*, *13*, 759–774.

Nolan, J. P. (1999), Univariate stable distributions: Parameterization and software, in *Practical Guide to Heavy Tails: Statistical Techniques and Applications*, edited by R. J. Alder, R. E. Feldman, and M. S. Taqqu, pp. 527–533, Springer, New York.

Oberbeck, V. R. (1971), Implications of regolith thickness in Apollo 16 landing site, *NASA Tech. Memo. TM X-62089*, NASA, Washington, D. C.

Pieters, C. M., J. B. Adams, P. Mouginis-Mark, S. H. Zisk, M. O. Smith, and J. W. Head (1985), The nature of crater rays: The Copernicus example, *J. Geophys. Res.*, *90*, 12393–12413.

Pike, R. J. (1974), Ejecta from large craters on the Moon: Comments on the geometric model of McGetchin et al., *Earth Planet. Sci. Lett.*, *23*, 265–274.

Quaide, W. L., and V. Oberbeck (1975), Development of the mare regolith: Some model considerations, *Moon*, *13*, 27–55.

Rhodes, J. M. (1977), Some compositional aspects of lunar regolith evolution, *Philos. Trans. R. Soc. London, Ser. A*, *285*, 293–301.

Samorodnitsky, G., and M. S. Taqqu (1994), *Stable Non-Gaussian Random Process*, CRC Press, Boca Raton, Fla.

Schultz, P. H. (1988), Cratering on Mercury: A relook, in *Mercury*, edited by F. Vias, C. R. Chapman, and M. S. Matthews, pp. 275–335, Univ. of Ariz. Press, Tucson.

Schultz, P. H. (1999), Ejecta distribution from oblique impact into particulate targets, *Lunar Planet. Sci.* [CD-ROM], *XXX*, abstract 1919.

Schultz, P. H., and J. F. Mustard (2004), Impact melts and glasses on Mars, *J. Geophys. Res.*, *109*, E01001, doi:10.1029/2002JE002025.

Schultz, P. H., D. Orphal, B. Miller, W. F. Borden, and S. A. Larson (1981), Multi-ring basins formation: Possible clues from impact cratering calculations, *Proc. Lunar Planet. Sci. Conf.*, *12A*, 181–195.

Settle, M., and J. W. Head (1977), Radial variation of lunar crater rim topography, *Icarus*, *31*, 123–135.

Shoemaker, E. M., E. C. Morris, R. M. Baston, H. E. Holt, K. B. Larson, D. R. Montgomery, J. J. Rennilson, and E. A. Whitaker (1969), Television observations from Surveyor, in Surveyor Program Results, *NASA Spec. Publ.*, *NASA SP-184*, 19–128.

Shoemaker, E. M., M. H. Hait, G. A. Swann, D. L. Schleicher, G. G. Schaber, R. L. Sutton, D. H. Dahlem, E. N. Goddard, and A. C. Waters (1970), Origin of lunar regolith at Tranquillity base, *Proc. Apollo 11 Lunar Sci.*, *Conf. 3rd, Geochim. Cosmochim. Acta Suppl. 1*, 2399–2412.

Simon, S., J. J. Papike, and J. C. Laul (1981), The lunar regolith: Comparative studies of Apollo and Luna sites, petrology of soils from Apollo 17, Luna 16, 20, 24, *Proc. Lunar Planet. Sci. Conf. 12B*, 371–388.

Simon, S. B., J. J. Papike, D. C. Gosselin, J. C. Laul, S. S. Hughes, and R. A. Schmitt (1990), Petrology and chemistry of Apollo 17 regolith breccias: A history of mixing of highland and mare regolith, *Proc. Lunar Planet. Sci. Conf. 20th*, 219–230.

Staid, M. I., C. M. Pieters, and J. W. Head (1996), Mare Tranquillitatis: Basalt emplacement history and relation to lunar samples, *J. Geophys. Res.*, *101*, 23,213–23,228.

Stöffler, D., D. E. Gault, J. A. Wedekind, and G. Polkowaski (1975), Experimental hypervelocity impact into quartz sand: Distribution and shock metamorphism of ejecta, *J. Geophys Res.*, *80*, 4062–4077.

Swann, G. A., et al. (1971), Preliminary geologic investigations of Apollo 14 landing site, Apollo 14 preliminary science report, pp. 39–86, Sci. and Tech. Inf. Off., NASA, Washington, D. C.

Watkins, J., and R. Kovach (1973), Seismic investigation of the lunar regolith, *Proc. Lunar Sci. Conf. 4th*, 2561–2574.

Wilhelms, D. E. (1987), The Geological History of the Moon, *U.S. Geol. Surv. Prof. Pap.*, *1348*, 1–245.

Wood, J. A., J. S. Dickey, U. B. Marvin, and B. N. Powell (1970), Lunar anorthosites and a geophysical model of the moon, *Proc. Apollo 11 Lunar Sci. Conf 3rd., Geochim. Cosmochim. Acta Suppl. 1*, 965–988.

Yingst, R. A., and J. W. Head (1999), Geology of mare deposits in South Pole-Aitken basin as seen by Clementine UV/VIS data, *J. Geophys. Res.*, *104*, 18,957–18,979.

Ziegler, R. A., L. A. Haskin, R. L. Korotev, B. L. Jolliff, and B. L. Jolliff (2003), The Apollo 16 mare component: Petrology, geochemistry, and provenance, *Lunar Planet. Sci.* [CD-ROM], *XXXIV*, abstract 1454.

Ziegler, R. A., R. L. Korotev, B. L. Jolliff, L. A. Haskin, and J. Gillis (2004), Apollo 16 mafic glass: Geochemistry, provenance, and implications, *Lunar Planet. Sci.* [CD-ROM], *XXXV*, abstract 2082.

Zolotarev, V. M. (1986), *One-Dimensional Stable Distribution*, *Transl. Math. Monogr.*, vol. 65, Am. Math. Soc., Providence, R. I.

L. Li, Department of Geology, Indiana University–Purdue University at Indianapolis, 723 West Michigan Street, Indianapolis, IN 46202, USA. (ll3@iupui.edu)

J. F. Mustard, Department of Geological Sciences, Brown University, Providence, RI 02912, USA.